

Article

Environmental Impact Assessment of the Subsurface in a Former W-Sn Mine: Integration of Geophysical Methodologies

Hender De Almeida ^{1,*}, Maria Cristina Gomes Marques ², Helena Sant'Ovaia ³, Rui Moura ¹ and Jorge Espinha Marques ³

¹ Departamento de Geociências, Ambiente e Ordenamento do Território, Faculdade de Ciências, Universidade do Porto, Rua do Campo Alegre, 687, 4169-007 Porto, Portugal

² Sixense, Rua do Batalheiro, nº 39, 2580-061 Alenquer, Portugal

³ Instituto de Ciências da Terra, Universidade do Porto, Rua do Campo Alegre, 687, 4169-007 Porto, Portugal

* Correspondence: up202008625@edu.fc.up.pt

Abstract: Associated with the exploitation of metallic minerals in Europe during the 20th century, several mining areas were abandoned without adequate environmental intervention. Furthermore, these areas lack studies to characterize the impact of pollution on the hydrogeological system. The area surrounding the tungsten mine of Regoufe, in northern Portugal, is one such area exploited during the Second World War. The accumulation of sulfide-rich tailings may have caused an acid mine drainage (AMD), where the leaching processes caused by seepage water led to soil contamination, evidenced by its acid character and anomalous concentrations of some Potentially Toxic Elements (PTE) reported in previous studies. The present research proposes an innovative approach that seeks the integration of different geophysical techniques to characterize the impact of mining activity on the subsurface. Electrical resistivity (ER) and electromagnetic (EM) were used to measure subsurface electrical properties. In addition, seismic refraction and Multichannel Analysis of Surface Waves (MASW) were performed to characterize the geometry, depth, and geomechanical behavior of the soil and rock bodies. The integration of these techniques allowed the interpretation of hydrogeological sections and a 3D resistivity volume to gain insight into the distribution of potentially contaminating fluids and tailings material present in the mining valley.

Keywords: refraction seismic; MASW; electromagnetics; electrical resistivity; pollution; mining



Citation: Almeida, H.D.; Gomes Marques, M.C.; Sant'Ovaia, H.; Moura, R.; Espinha Marques, J. Environmental Impact Assessment of the Subsurface in a Former W-Sn Mine: Integration of Geophysical Methodologies. *Minerals* **2023**, *13*, 55. <https://doi.org/10.3390/min13010055>

Academic Editor: Giovanni Martinelli

Received: 29 November 2022

Revised: 19 December 2022

Accepted: 20 December 2022

Published: 28 December 2022



Copyright: © 2022 by the authors. Licensee MDPI, Basel, Switzerland. This article is an open access article distributed under the terms and conditions of the Creative Commons Attribution (CC BY) license (<https://creativecommons.org/licenses/by/4.0/>).

1. Introduction

Accompanying the extensive exploitation of mining resources in the northern part of Portugal, large areas of accumulation of waste materials from the extraction process were generated over several decades of the 20th century. Due to the lack of environmental intervention in the development and deactivation phases of the mines, these accumulations can cause significant contamination of the soil, water, and air around the mining areas [1–4]. In this sense, the present research work focuses on the Mining Area of Regoufe in the Arouca Council. These mines exploited quartz veins mineralized in tungsten and cassiterite, ceased their extractive activity in the late 1970s of the twentieth century, and the environmental intervention was almost null after mine closure.

There are several regions in Europe where mining activities in the past have had a major impact on the environment [5–8]. Many of these cases are associated with metalliferous mining deposits whose ores may contain abundant sulfides. The mining process allows these sulfides to be in direct contact with an oxygenated environment. Thus, during mining, there are a number of interventions, such as waste rock dams; waste rock piles; leachate piles; low-grade ore stockpiles; open pit floors and; and other rock excavations. When these sulfides are exposed to the atmosphere or oxygenated groundwater, these sulfides oxidize and produce acidic water rich in sulfates, heavy metals, and metalloids, generating a major

cause of pollution in the mining industry known as “acid mine drainage” (AMD) [9]. From these deposits, high concentrations of metals and salts affect surface water, aquatic life, sediments, and groundwater. Often, DAM mines have a greater impact on groundwater than surface water, which can come from tailings dumps, tailings, contaminated soils, etc. [10,11]. These flows subsequently pass into aquifers, especially if the waste deposits are uncovered [12]. In the case of metalloids, they move slowly, creating different pH zones in the contamination plume [9].

The study area is close to the village of Regoufe, with crop and pastoral areas, as well as the insertion of the mining area in the geopark system in Portugal [13]. It is important to conduct characterization studies to assess the environmental impact left by the mining activity, being the main target of this project, the analysis of soils, subsoils, and groundwater in the area surrounding the mine. In this context, considering the application of mitigation or remediation measures, the focus of this research was the characterization of the hydrogeological system in the areas covered by the Regoufe mine. Using integrated geophysical techniques to try to establish the spatial distribution of contaminated areas in the subsurface and support these results with the surface physicochemical observations, allowing to strengthen of the proposed model.

The process of geophysical quantification has been very relevant for hydrogeological characterization in environmental studies [14,15]. It is increasingly widely accepted in the scientific community that the integration of results by combining different sources of information makes the geological model more robust and credible [16,17]. Given the high geological complexity and relatively little information that can be obtained by direct subsurface methods, it is increasingly imperative to obtain data from different sources to maximize information and develop a higher-resolution geological characterization [16]. Integration of subsurface geophysical data and laboratory analyses allowed us to establish relationships between the electrical properties of the subsurface and observations in both soil and water samples. The electrical properties are characterized by low conductivity in soils of coarse-grained gravel deposits, fine-grained deposits of quartzitic nature, and in the granitic substrate. In contrast, there is high conductivity in areas of water presence associated with interflow zones or as a response from the saturated zone. The geophysical integration using techniques such as seismic refraction and MASW allowed a better characterization of the thickness of the mine waste deposits and differentiation of the granitic zone with a major alteration and depth of the granitic substrate. In an attempt to understand the electrical behavior of hypothetical AMD, several scenarios were carried out in the laboratory using bottled water samples with higher mineralization than the samples collected from the mine drainage gallery. Integration of the ERT and EM electrical data reflects a central area of the mine valley with values of about 1000 Ωm , which are much higher when compared to higher mineralization scenarios from laboratory measurements. These results suggest a low probability of ionized water occurring and, therefore, low levels of underground water contamination. Finally, in order to characterize the mine waste deposits and the definition of the water table surface in the mine of Regoufe, four vertical sections, a 3D model of electrical resistivities, and a conceptual hydrogeological model were constructed.

The importance of understanding the hydrogeological system has been highlighted in abandoned mine sites in previous research [18,19], where the main objective was fundamentally mineral exploitation. Former mine areas where mining activity stopped without any remediation processes have been benefiting from hydrogeological modeling [19], and comprehension of the hydrogeological system has permitted to proposal mitigation work on tailings and galleries drainage sites. Despite the high uncertainty in regions of crystalline systems, this type of integrated modeling provides a basis for an unprecedented conceptual model in the Regoufe mining area, as well as future more detailed analyses of the hydrogeological system around the mining area. As well as defining appropriate environmental intervention work, such as soil remediation and treatment of potentially contaminated water.

2. Geological Setting

From the geotectonic point of view, the studied area integrates the western part of the region called the Central Iberian Zone, which occupies the central part of the Iberian Massif (Figure 1). The region comprises the domain associated with the stratigraphic subdivision initially known as the “Complexo Xisto-grauvuico” [20,21]. In the Precambrian or Lower Cambrian, during a distensive regime with sedimentation in a context of tectonic instability, a basin was established and allowed a powerful accumulation (8000–11,000 m) of siliciclastic materials [22,23]. The Hercynian Belt was formed in the late Upper Paleozoic due to the collision of two large continents, Laurasia and Gondwana, and smaller continental masses named Avalonia and Armorica [24–27]. This deformation results from the action of a more or less continuous succession of three tectonic phases followed by a final stage of the Hercynian orogeny of more brittle characteristics [28,29]. More recent research shows that the installation of most Hercynic granites is related to the 3rd deformation phase, where the granitic pluton of Regoufe has been dated to 280 ± 9 Ma by the Rb-Sr method [30].

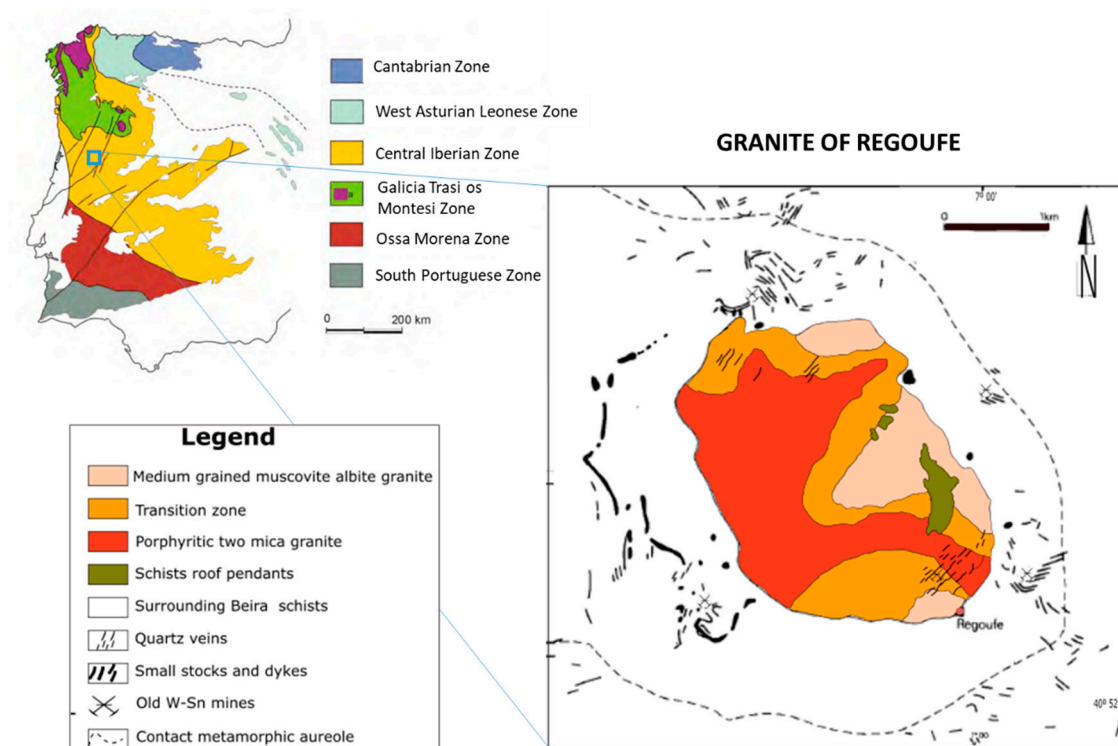


Figure 1. Geological sketch of the Central Iberian Zone modified with the location of the study area and its geological map, modified from [31,32].

The Regoufe granite is a small pluton with an outcrop extension of approximately 6 km^2 with a slightly elongated circular geometry in an NW-SE direction. The granite presents a medium to coarse-grained porphyroid texture, mainly muscovitic, with the presence of scattered potassium feldspar megacrystals. The matrix is composed of feldspar, quartz, and muscovite showing a light color. The orientation of the feldspar megacrystals develops an NW-SE magmatic foliation which may suggest tectonic control during the installation of the granitic body. Tourmaline is a very common accessory with a few millimeters in length and black color; also, locally and dispersed, arsenopyrite crystals are observed surrounded by a halo of alteration [33]. The final stages of granitic intrusion were characterized by the circulation of hydrothermal fluids that allowed the precipitation of W-Sn minerals in quartz veins. These processes also produced the alteration of granite and metasedimentary rocks [34,35].

Analytical results show that the granite is extremely rich in Sn, W, Li, and Cs, rich in P, Ta, Rb, F, and U, about normal in Cu, Zn, and Nb, and low in Sr, Ti and Zr compared to global averages for granites low in calcium [31]. From the study by Sluijk [32], it was possible to conclude with respect to the mineralogy and geochemistry of the veins found there the following: Wolframite (Fe,Mn)WO₄ is the most abundant mineral, being richer in Mn than in Fe. Cassiterite (SnO₂) is developed in two generations, with crystals of different sizes. Several sulfides are also found, including arsenopyrite (FeAsS), pyrite (FeS₂), and sphalerite (ZnS). Note that arsenopyrite is associated with cassiterite. In some very thin veins, the predominant sulfide is sphalerite. Pyrite is one of the last minerals to crystallize and is not very frequent, as well as bismuthinite. With respect to gangue, there are silicate minerals such as quartz, muscovite, beryl, and apatite. Supergene alteration products include scorodite, limonite, autunite and bindheimite [32,36].

3. Materials and Methods

The environmental impact assessment of the mining activity in Regoufe has been developed in several research works in the last 12 years. Several sources of geological, geochemical, and geophysical data have been obtained to determine the contamination potential and the affected areas [1,2,4,36–38]. Much of the information collected was interpreted for specific purposes, such as assessing the degree and type of contamination in surface water, soils, and organic matter. In the present work was considered the use of different geophysical techniques that address particular physical principles to complement the results of the diverse methodologies were considered, and thus mitigating the limitations in each of them and strengthen the results of the presented subsurface model (Figure 2).

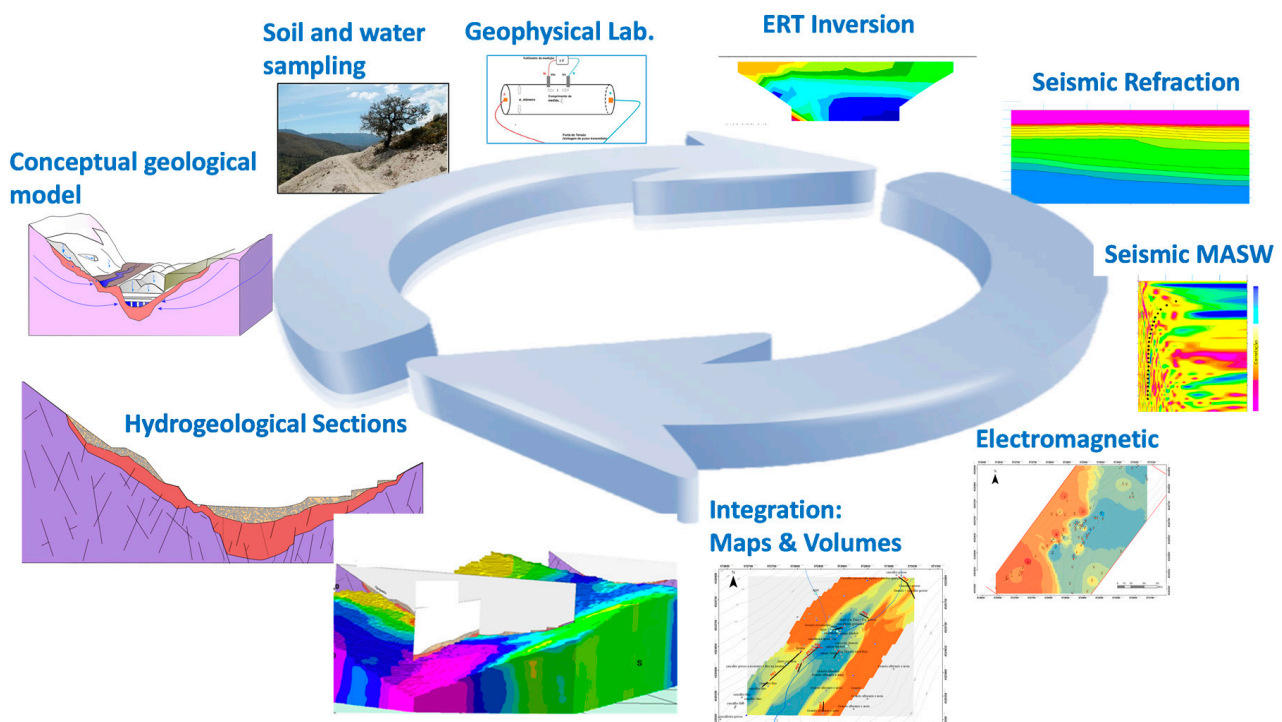


Figure 2. Integrated methodology of geophysical methods proposed in this study.

Since geophysical techniques comprise the measurement of physical properties of the rock–fluid system, such as seismic wave propagation velocities, resistivity, or electrical conductivity of the materials, it is essential to correlate such geophysical properties with geological properties such as rock type or soil material, existing fluids, mineralogical content, etc. In this sense, the proposed methodology seeks to integrate data of higher vertical resolution given by soil samples to try to predict their behavior in areas with

electrical profiles with subsoil information and to extrapolate in 3D based on the EM data as a controller of the regional variations observed. In this respect, the present work considered the resolution and working scale of the different tools, the ease of operation, and the time to collect the data. Based on direct measurements, it was used soil sampling in the field was used, and laboratory measurements of high vertical resolution (cm) and shallow depth of investigation (cm) were obtained. Then, their integration with ERT electrical profiles with greater depth of investigation (5 to 15 m), although with a lower vertical resolution (0.25 to 1.25 m); later, use of seismic information to validate the bedrock model thickness of the mine landfills bodies and perform a structural-constrained ERT inversion in order to improve the image of the different layer's boundaries. Finally, these results were extrapolated in the area with the poorer vertical resolution data given by the electromagnetic EM technique (3 to 6 m) but with greater spatial coverage and used to obtain a regional framework of the subsurface geoelectrical behavior.

4. Results

4.1. Previous Studies on Water and Soil Samples

In the combined works of Correia [1] and Favas [37], physicochemical analyses (temperature, pH, Eh, and electrical conductivity (EC) of the water in Regoufe and surrounding areas were carried out. These studies conducted sampling campaigns at the exit points of the galleries, runoff from the tailings [1,36,37], and water lines along the mine [1]. The results obtained showed an acid character close to the neutrality of these waters, the most acidic those near the galleries and waste piles (pH 4.75–6.46 [1], in the case of water lines and downstream areas of the mine, the pH value is lower (5.35 in water lines) [1]. Further studies were conducted with regard to the water, Durães et al. [2] point out that it presents pH values close to neutrality, between 5.99 and 6.88 [2,4]. Durães [2] highlights the low values of PTE, i.e., Mn (1.04–13.6 µg/L), Zn (19.6–484 µg/L), Cd (0.04–9.45 µg/L) and As (0.78–206 µg/L). The work done jointly by Sousa [4] and Durães [2] included not only water but also soil analyses. The study covered the region around the mine and included agricultural areas near the village of Regoufe. In these studies, natural soils, agricultural soils, and waste materials were characterized as being acidic to very acidic [2,4]. Despite the characteristic of acidic soils, the electrical response is anomalous, obtaining very low values of conductivity (between 7.8–158 µS/cm). In addition, these authors make a statistical description highlighting the presence of Potentially Toxic Elements (PTE) with high values mainly of As and Cd, which are higher in the surrounding areas of the mine, especially in the quarry site, although in the surrounding agricultural areas, although lower, they also show high contamination levels.

Given these uncertainties regarding acidic soils/waters close to neutrality and the multiple scenarios of PTE enrichment of the surrounding soils, it is necessary to try to reproduce the actual contaminant transport mechanisms through integrated models that combine geochemical, geological, and geophysical information to evaluate the link between the contamination sources, the surface, and subsurface drainage network and the anomalous zones with deposition of pollutant elements. This type of study can lay the foundation for a hydrological fluid circulation model to apply similar methodologies in mining areas and assess their environmental impact, especially regarding water and soil resources.

4.2. Laboratory Electrical Resistivity Results

By taking advantage of the effect of the ionizing character present in water on the electrical properties, resistivity measurements were carried out in the laboratory with water obtained from mine galleries, bottled water, and mixtures of two different types of soil from the piles and saturated with the before mentioned fluids. The objective of this activity is, first, to establish ranges of minimum observable resistivity values. Second, to evaluate the effect of water type on measured electrical resistivities, and finally, to estimate the variation in electrical response between different soil types. With these parameters established, the

goal is to attempt to reproduce hypothetical underground scenarios and thus evaluate the different electrical responses using the mined material.

For these analyses, two soil samples and one water sample were collected from the mine drainage gallery in February 2022 (Figure 3). In addition, bottled water samples were used: “Serra da Estrela” spring water and “Frize” mineral water, whose physicochemical characteristics provided by the bottling companies are shown in Table 1, where it is shown that the groundwater from the mine drainage gallery has the lowest mineralization. With regard to the resistivity values obtained, the following observations should be noted:

- The mine drainage gallery water has significantly higher resistivities (441 Ωm) than bottled water with higher salt concentrations (“Frize,” 4 Ωm);
- The mine drainage gallery water has slightly higher resistivities (441 Ωm) than the bottled water with low mineralization (“Serra da Estrela,” 298 Ωm);
- In the cases with the two types of soil matrices (fines tailings and other inert ore materials) saturated with mine drainage gallery water, the resistivity response is equivalent and of the same order of magnitude (693 Ωm and 785 Ωm respectively);
- For soil saturated with saline water (mineral water “Frize”), the resistivity values are quite low (31 and 29 Ωm for both soil types) compared to the responses of soil saturated with mine drainage gallery water (with a difference of one order of magnitude).

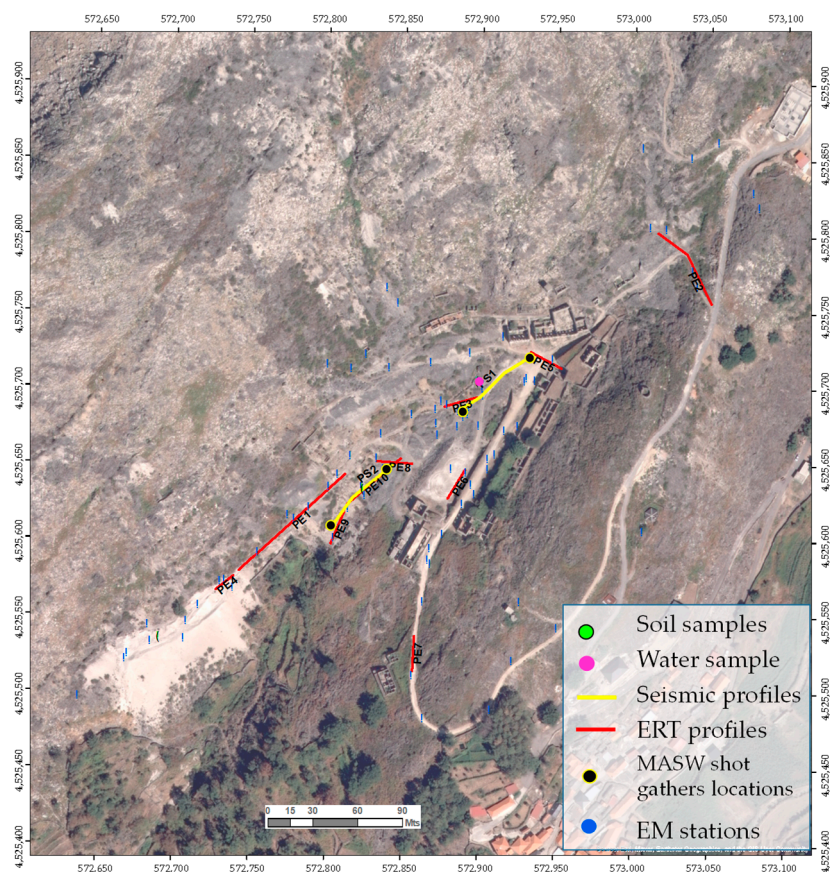


Figure 3. Location of soil and water samples, electrical resistivity transverse profiles (ERT), electromagnetic stations (EM), and profiles used for seismic refraction and MASW analysis.

These results first indicate, as expected, a decrease in resistivity as ionic concentrations in the fluid solutions increase. In addition, the observation that there is a strong effect of the ionizing capacity of the waters on the samples of the soil-fluid system, decreasing up to one order of magnitude the observed resistivities, as noted in the case of groundwater with high ionic content.

Table 1. Chemical composition of waters used in the laboratory to measure the electrical resistivity of “Frize” mineral water, “Serra da Estrela” spring water, and water from a mine drainage gallery in Regoufe.

Parameter	pH (20 °C)	SiO ₂	Cl ⁻	F ⁻	HCO ₃	Na ⁺	Mg ²⁺	Ca ²⁺
Unit		mg/L	mg/L	mg/L	mg/L	mg/L	mg/L	mg/L
Parametric value ¹	6.5 ≤ pH ≤ 9.5	-	250	1.5	-	200	-	-
Frize	6.14 ± 0.23	3090 ± 340	122 ± 12	1.9 ± 0.5	2100 ± 250	635 ± 82	31.4 ± 5.2	106 ± 29
Serra da Estrela	5.8–7	17 ± 5.5	3.2 ± 0.9	-	16.5 ± 8	4.4 ± 1.1	-	2.7 ± 1.6
Mine drainage gallery ²	6.01	-	4.17	-	2.21	2.84	0.32	1.01

¹ Parametric value according to the Directive (EU) 2020/2184 of the European Parliament and of the Council of 16 December 2020 on the quality of water intended for human consumption. ² Sample taken on February 2022, data provided by Catarina Mansilha, personal communication, 2022.

4.3. Electrical Resistivity Traverse Profiles (ERT)

The electrical profiles used in this study combine different surveys carried out between 2017 and 2022 in different seasons of the year (Figure 3). The PE1 (Figure 4) and PE2 (Appendix A) profiles are the longest and deepest in this study, and 48 electrodes were used arranged using Wenner-type geometry with spacings of 2 m for the PE1 profile and 1.25 m for the PE2 profile. Both PE1 and PE2 covered a more extensive zone in the western and northeastern parts of the mining area, respectively. The remaining profiles are shorter and shallower, as their purpose was to assess the potential for contamination in the gallery areas and mine tailings zones with spacing between 1.5 and 3 m and lengths between 22.5 and 45 m. These profiles were conducted to evaluate soils in pile zones (PE3, PE8, PE9, and PE10, Appendices A and B), zones near gallery exits (PE5, Appendix A), reference zones with an outcropping of granitic zones (PE7, Appendix B) and disposal of materials in zones relatively far from the galleries (PE6, Appendix B).

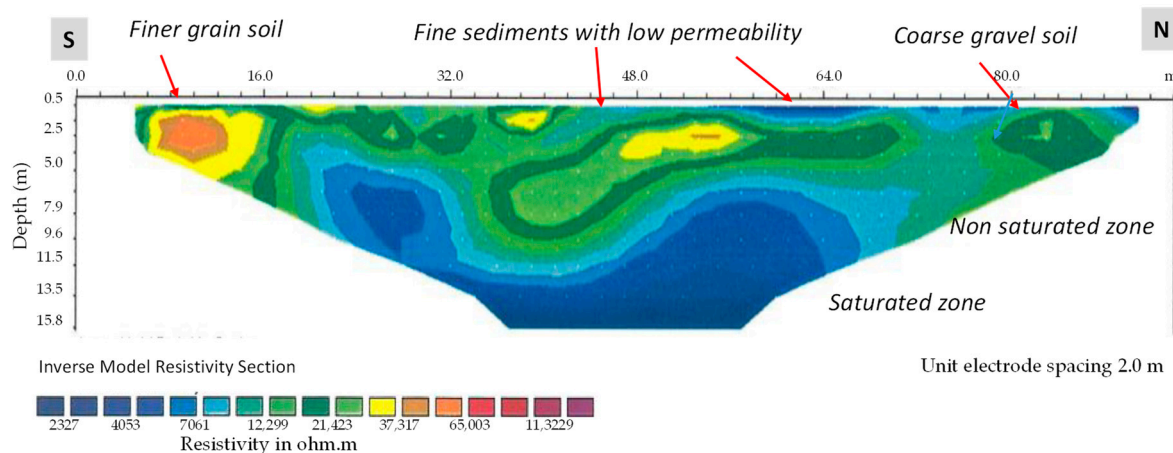


Figure 4. Interpreted Electrical Resistivity Profile (ERT) PE 1. Look at Figure 3 for profile location.

In general, the results of the profiles performed in the acquisition campaigns present results that show some more resistive zones near the surface and notably with lower resistivities in the deeper levels (Figure 4). This behavior is to be expected considering the existence of watercourses in the valleys and gallery areas, which cause the dissolution of the residual material of the tailings, making them an excellent electrolytic conductor. On the other hand, the areas closer to the surface, with disaggregated material and low moisture content, are poor conductors.

In particular, profiles PE2 and PE7 clearly show highly resistive zones that tend to become more resistive at deeper levels (4 m in PE7 and 9 m in PE2). This observation is consistent with the existence of granite outcrops in the northeastern part of profile PE2 and extending southward beyond the extent of profile PE7. Since the effect of weathering

is greatest at the surface, it can be interpreted that at deeper levels, the granite is less altered, and therefore there are fewer pore spaces containing electrolytes, which justifies the increased resistivity. Similar examples of granites in the equivalent geological context in Portugal are referred to, characterizing zones of the granitic substrate with little fracturing in zones with resistivities higher than 3000 Ωm [39].

In the case of the profiles in the central part of the valley or in the areas close to the galleries, the influence of the presence of water is remarkable. As observed in the laboratory tests, the electrical response is mainly conditioned by water saturation, so in the cases of profiles PE3, PE5, PE8, and PE9, it was not possible to differentiate the material present in the subsurface and it was only possible to analyze the results with respect to the groundwater ionic potential. As an example, the profile PE1 shows three intervals with quite distinct electrical responses observed. A shallow zone (depths below 5 m), where the northern zone appears less resistive consistent with a heterogeneous zone with the presence of coarse gravels (relatively high resistivity between 12,000 and 21,000 Ωm) and finer sediments with low permeability and high-water saturation (resistivity between 3000 to 7000 Ωm) (Figure 4). At the same time, the southern zone presents fine material, with good sorting and high permeability, with high electrical resistivity (between 25,000 and 65,000 Ωm). An intermediate zone (depths between 5 m to 11 m) shows lower resistivity than the shallow zone and are interpreted as higher water saturation levels (between 4000 and 25,000 Ωm) is probably associated with the non-saturated zone. Finally, a deeper interval, with the lowest resistivity range (between 1000 and 4000 Ωm) is likely associated with the saturated zone.

4.4. Integration of Electrical Resistivity Data (Laboratory Data and Field Profiles ERT)

The resistivity values observed in the deeper zones of the electrical profiles are relatively higher (2000–3000 Ωm) than the waste material with mine drainage gallery water-saturated measured in the laboratory (700 Ωm). Still, these values are much lower than the minimum values of a saturated granite (4500 Ωm) according to Telford [40], so the reported values (between 2000 and 3000 Ωm) can be considered as due to a weathered and saturated granitic rock or a saturated conglomerate (2000 Ωm) as described in the same study [40]. Saprolites, according to Palacky [41], are highly weathered granitic rocks presenting much lower values (below 200 Ωm), and therefore the zones observed in this range (2000–3000 Ωm) can be considered granites with a low degree of alteration. In this sense, it is interpreted that the deeper zones should present either water-saturated quarry material (mechanically equivalent to a conglomerate or gravel) or a slightly weathered, water-saturated granite.

When compared, the resistivity values obtained in the laboratory for saline water (commercial “Frize” water) are an order of magnitude lower (30 Ωm) than that observed in the electrical profiles (minima of 400 Ωm in profile PE10, in the others, minima of 2000 Ωm). These results indicate a rather low probability of occurrence of saturated soils with acidic water in the studied area.

4.5. Electromagnetic Surveying Results (EM)

In the development of the present research, a device manufactured by Geonics Lmt, EM31 series, was used, which is considered a dual coil moving source device with wide use in environmental engineering. The EM31 device is calibrated to measure the correct conductivity when the subsoil is uniform so that if layers with different electrical properties exist, the equipment will read an intermediate value. The procedure comprises EM field measurement of the vertical component (dV) and the horizontal component (dH).

Relative EC maps are shown in Figure 5a for the horizontal dH (investigation depth to 3 m) and Figure 5b for the vertical dV (investigation depth to 6 m) components, respectively. These results can be used to obtain relative conductivity measurements and to observe the trend of the hydrogeological background. Both maps show a relative increase in conductivities in the southern and eastern parts of the study area. The southwestern areas,

when compared to other areas of the mine, correspond to fine residues composed of quartz. In the case of the more superficial intervals (less than 3 m deep), they may present humified organic matter (HOM). The reduced EC may be due to both the presence of this HOM and the high hydraulic conductivity, as both factors reduce the water content. At the deeper levels (between 3 and 6 m), the material will be hydrophilic, but the high hydraulic conductivity facilitates vertical percolation, so the moisture content will also tend to be reduced, showing values of relatively low EC, slightly higher than at the more superficial levels. When comparing the electrical results in granitic zones and coarse debris material, it is not possible to discriminate these responses in the EM data (for both dV and dH).

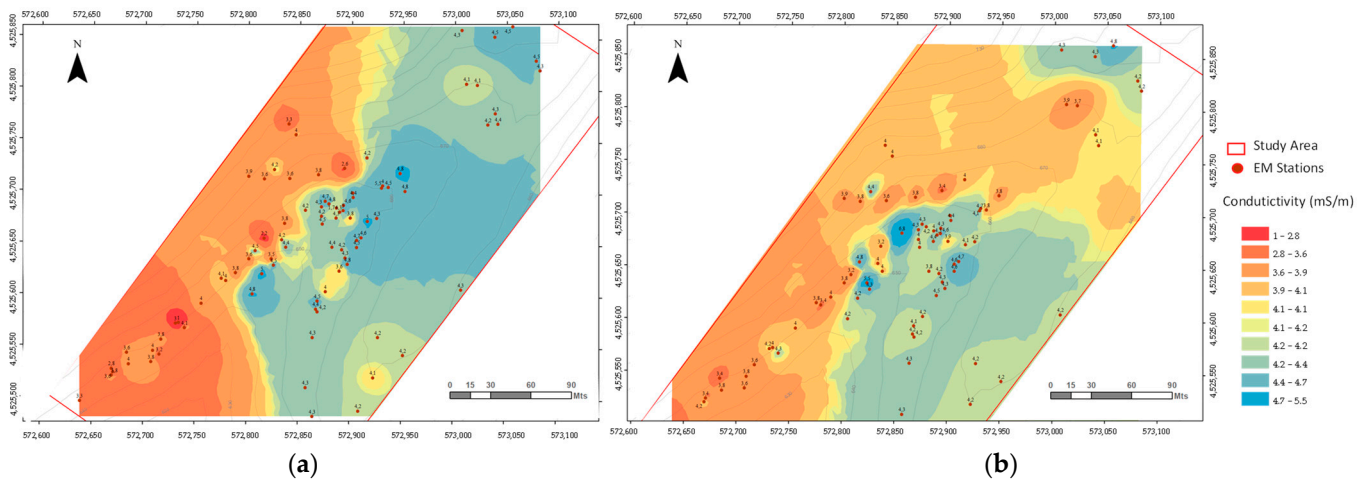


Figure 5. Relative electrical conductivity (EC) maps for: (a) Horizontal component dH (research depth to 3 m); (b) Vertical component dV (mS/m) (research depth up to 6 m).

The dH horizontal conductivity map shows more heterogeneity, which is an expected result due to the greater influence of soil or rock types and less influence of groundwater, contrary to the case of the dV vertical conductivity map where the influence of the wetland is greater, as is notable in the southern, eastern and northeastern zones in the dV vertical conductivity map (zones in blue).

4.6. Seismic Surveying Results

Regarding the seismic survey in the Regoufe mining area, two profiles were performed in order to obtain information about compressional and shear wave velocity distribution using refracted waves and surface waves. Both profiles were performed in the central region of the mine, specifically in the valley area with an accumulation of coarse gravel and fine material (Figure 3). The objective of these profiles was to evaluate the possibility of obtaining the thickness of the rejected material, detect the depth of the water table and analyze the mechanical behavior of the seismic waves in order to detect possible lithological contacts. For this survey, the following equipment was used: a 24-channel seismograph, a metal plate, a sledgehammer that acts as a seismic source, a trigger, and a tape measure to establish the location of the shots and detectors. The 12 detectors, 4.5 Hz geophones, were interspersed every 5 m, with the first detector placed 2.5 m from the first shot. For the seismic refraction analysis, several shots were taken and placed at 0 m, 15 m, 30 m, 45 m, and 60 m. For the MASW analysis was used the same data was acquired for the seismic refraction analysis, taking only those shots located at 0 m and 60 m from each seismic profile.

4.6.1. Seismic Refraction Results

The results for seismic profiles PS1 and PS2 are illustrated in Figure 6A,C, respectively. Seismic waves with different velocities were identified, i.e., direct waves (red lines), two refraction interfaces in the case of profile PS1 (green and blue lines), and only one refraction

interface in the case of profile PS2 (green lines). Once the velocity selection is validated, an initial 2D model of layers along the profile is generated. From this initial velocity model, a tomographic inversion process is performed in order to obtain a 2D profile, which honors the arrival time data and minimizes the errors for the constructed grid. In this case, 10 layers and a maximum depth of the PS1 profile of 20 m and for the PS2 profile of 12 m were defined. The p-wave velocity modeling results for profiles PE1 and PE2 are illustrated in Figure 6B,D, respectively.

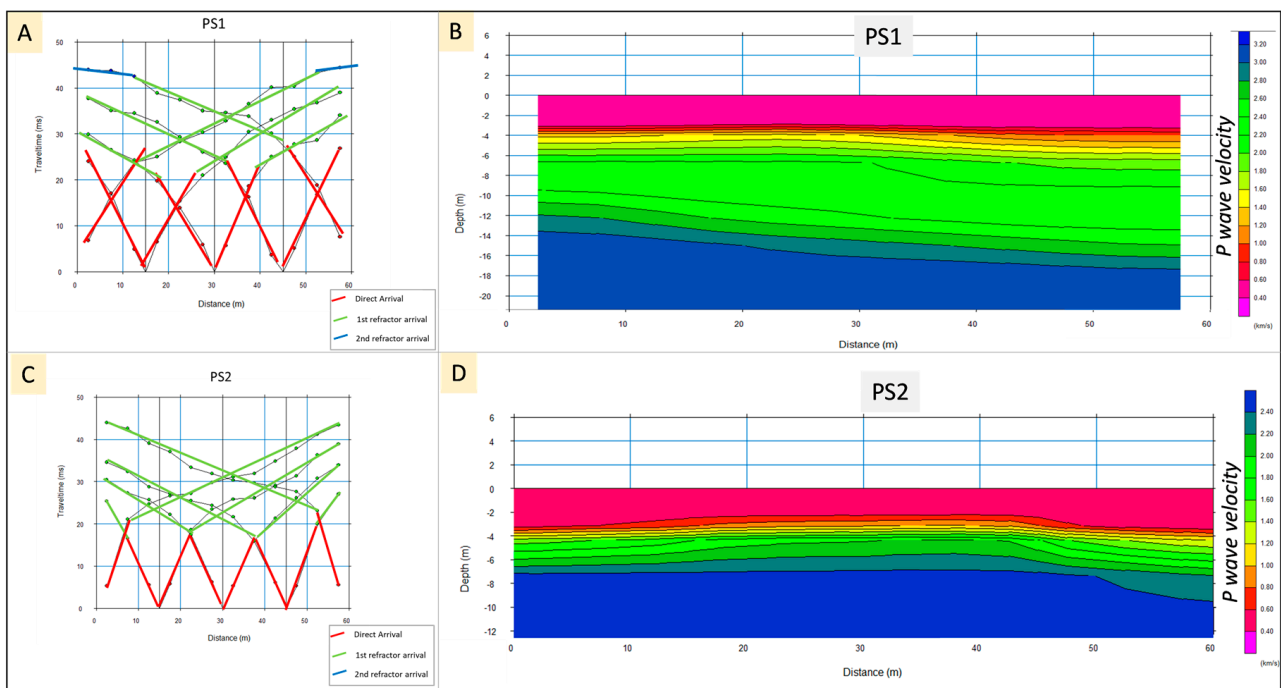


Figure 6. Graphs of travel time vs distance and refracted branches velocities for (A) Seismic profile PS1; (C) Seismic profile PS2. P-wave velocity model obtained by the tomographic inversion process for (B) Profile PS1; (D) Profile PS2.

4.6.2. Multi-Channel Analysis of Surface Waves Results (MASW)

Based on the surface wave analysis, the MASW method was applied to analyze the shear wave velocity of the more superficial layers in the central valley area with mound deposits at Regoufe (Figure 3). First, an analysis of the seismic records corresponding to the shots located at 0 m and 60 m from each seismic profile was performed. The seismic data are converted from the time-distance domain to the frequency-phase velocity domain through Fourier transforms or “apparent velocity spectra” (Figure 7A).

For profiles PS1 and PS2, two dispersion curves are obtained for both the source at 0 m and 60 m. In the last step, the vertical “s” wave velocity profiles are obtained by inversion modeling based on the data and optimizing the initial layer model. In this process, the following parameters are set: the number of layers and the maximum depth of the model. Figure 7B shows the 1D model results from MASW, particularly “s” wave velocity for 0 and 60 m of profile PS1, as well as “p” wave velocities (obtained from the seismic refraction inversion model). For comparison purposes and to evaluate the subsoil mechanically, an estimation of Young’s modulus E was carried out based on the “p” and “s” wave velocity data (extracted from seismic refraction and MASW inversion models, respectively), as well as the density of the material. In the case of density, values taken from the literature [40] were used. In this case, 2 gr/cc for the mine landfill soil and 2.6 gr/cc for the granitic substrate.

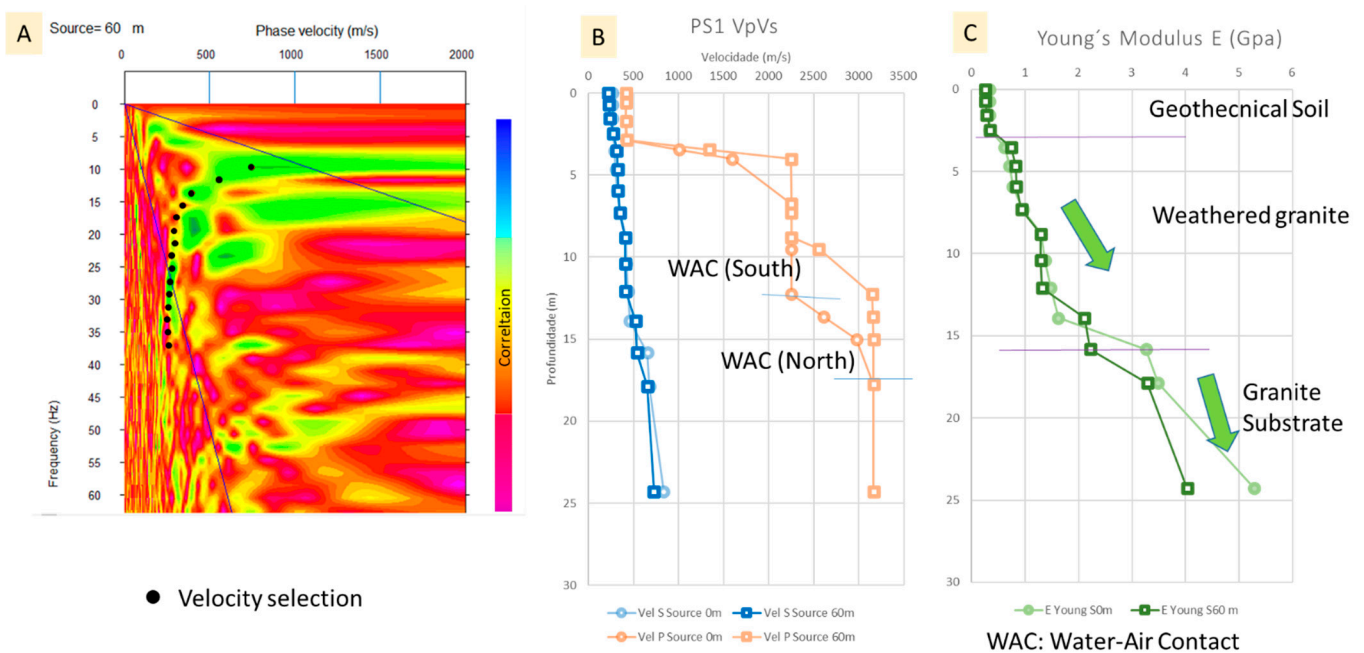


Figure 7. MASW results analysis in the PS1 profile (shots at 0m and 60 m): (A) Apparent velocity spectra and fundamental mode velocity selection (shot at 60 m); (B) P-wave (from seismic refraction) and S-wave (MASW) velocity curves; (C) Young's modulus "E" curves and its geomechanical interpretation.

The inversion models of the MASW data corroborate, on the one hand, the results obtained by the seismic refraction in relation to the thickness of the mine landfill soil, i.e., approximately 4 to 6 m (average shear wave velocity "Vs" of 254 m/s for PS1 and 215 m/s for the PS2 profile). From Young's modulus curves, it is possible to observe the changes related to the interface between the mine landfill soil and the granitic substrate when compared to the shear-wave velocities. The soil composed mainly of coarse-grained gravel reflects average values of 0.31 GPa for the PS1 profile and 0.25 for the PS2 profile. On the other hand, the granitic soil shows a gradual increase in this parameter in both profiles. However, from a depth of 15 m in both profiles, a change in slope is observed from an area with a significant increase in this parameter to an area with a low increment relative to deeper levels. This change in Young's modulus is interpreted as the transition from a more weathered (and therefore more ductile) granite to a zone with a stiffer granitic substrate (less fractured or less altered than the overlying zone) and, therefore, more homogeneous.

4.7. Integration of Seismic and Electrical Methods

In order to improve the geoelectrical image obtained with the conventional ERT methodology, this study used a geophysical process called structure-controlled inversion [42]. The particular case of this investigation involves the use of strong events associated with the top of the consolidated rock (bedrock), identified by seismic refraction and thus structurally delimiting the inversion of electrical resistivity data associated with the aquifer. The methodology and input information for the structure-controlled resistivity modeling is illustrated in Figure 8. From the estimated layer thicknesses observed in the seismic refraction in profile PS1 (Figure 8A), together with the measurement of apparent electrical resistivities in profile PE10 (Figure 8B) and topographic information (Figure 8C), the structure-controlled resistivity inversion modeling was performed (Figure 8D). The layers were divided from the profile shown in Figure 8A as "Interface 1" and "Interface 2", which represent the boundaries where the largest p-wave velocity contrasts were observed.

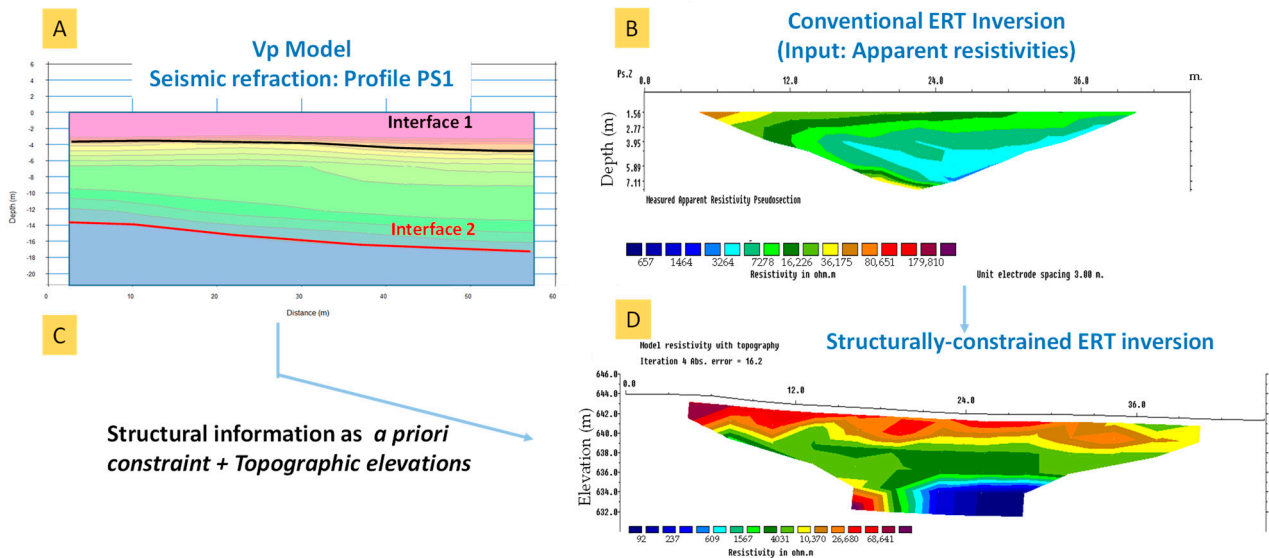


Figure 8. Input data and methodology used to perform an inversion of the structurally-constrained ERT inversion. (A) Definition of interfaces 1 and 2 with higher p-wave velocity contrast. (B) Input data of apparent resistivity (C) Topographic information and (D) Result of Profile PS1 using structurally-constrained ERT inversion.

The results of the structure-controlled inversion improved the conventional inversion process (Figure 9) since the boundaries in the latter appear blurred out and with low resolution (Figure 9A) so that the electrical properties of the layers can appear shifted and with smoother values.

As a result of the inversion, the difference in the electrical properties of the surface layer can be observed more clearly, with the presence of a greater heterogeneity with coarse gravels interspersed with intervals of finer material (Figure 9B). Incidentally, the relative decrease in resistivities in the zones of finer material to the south is still noticeable. While at the deeper levels (between 640 and 635 m a.s.l.), a more homogeneous zone is observed, which is interpreted as the unsaturated zone (resistivities of 4000 Ωm). This model also shows more clearly a flatter interface at approximately 635 m a.s.l., where resistivities decrease strongly (between 90 and 200 Ωm). These results indicate a significant reduction in resistivities compared to the previous modeling and compared to the rest of the profiles where highly saturated zones are interpreted (near the galleries with a minimum of 2000 Ωm ; see Figure 4). Furthermore, if compared to the results observed in the laboratory, where mineralized water was used, the values are close to highly ionized zones which suggest a potential zone of polluted water concentration in the deeper levels of this profile. Durães et al. [2] suggest in their work the possibility of migration of potentially contaminating PTE elements to deeper levels product of the leaching of tailings materials, and highlight the possibility of precipitation of metals contained in acidic waters in the form of sulfates, which are good conductors of electricity.

One of the limitations of this type of methodology is its conditioning on the interpretation of layer boundaries, so these results, which suggest a higher ionic concentration than reported in conventional models, must be corroborated with other electrical profiles or by applying other techniques such as electrical induction methods. Nevertheless, this methodology shows how the integration of seismic refraction results and resistivity profile data can help to better clarify lithological heterogeneities and to obtain a better resolution and definition of possible contaminated zones in the subsurface.

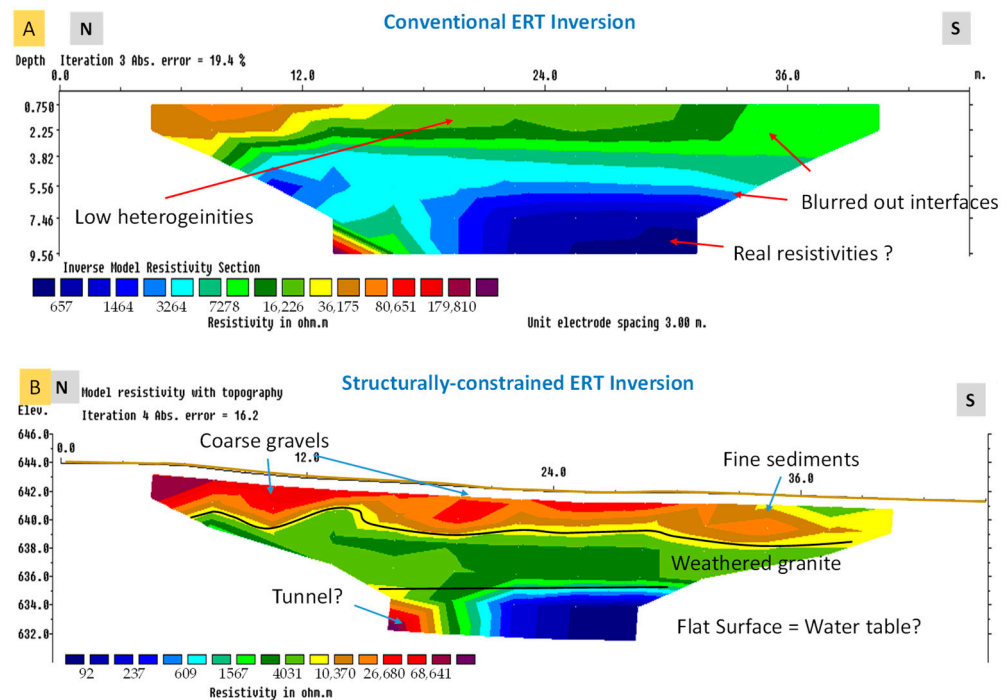


Figure 9. Results of the resistivity inversion of profile PE10 using (A) the conventional methodology and (B) the structure-controlled methodology.

4.8. Hydrogeological Conceptual Model and Representative Sections

In mountain areas, the development of groundwater distribution and circulation models—based on geology, geomorphology soil, climate, land use, and human activities—is a difficult task, even when relevant data are available [43–48]. However, a conceptual hydrogeological model is proposed for the Regoufe mining area considering information from field observations, aerial image interpretation, and subsurface geophysical measurements. It is important to note that the purpose of this study is not to generate a detailed hydrogeological conceptual model since that alone would be material for a separate project, but rather to provide a preliminary proposal of the hydrogeological system functioning based on subsurface geophysical and surface geology observations. This conceptual model will provide a starting point for future projects involving soil remediation and water treatment processes in areas affected by mining activities.

The hydrogeological conceptual model encompasses the unsaturated zone and the water table aquifer (Figure 10). Porous circulation media occur in the pedological soil and in the mining waste piles, whereas fractured circulation media correspond to the unweathered granite, and, finally, mixed circulation media occur in the weathered granite.

The mining waste piles were interpreted as the material of the highest hydraulic conductivity, while the weathered granite and the unweathered granite were interpreted as the material of intermediate and lowest hydraulic conductivity, respectively.

The depth to the water table varies with time and with the topographic position: (i) it is shallower during the wet season and deeper during the dry season; (ii) it is shallower in the valley bottom and deeper in the hilltops.

In the unsaturated zone, the circulation is mainly vertical, as water infiltrates and percolates until the water table. Yet, at the interface between geological materials of contrasting hydraulic conductivity, namely, between the weathered and the unweathered granite, interflow may occur during the wet season and originate in intermittent springs and streams. Except for the driest part of the year, the groundwater flow supplies part of the streamflow in a typical gaining stream context, whereas another part of the streamflow is supplied by the mine drainage galleries. Indeed, the existence of mine gallery systems tends to drain the rock mass and increase the streamflow in the surrounding region.

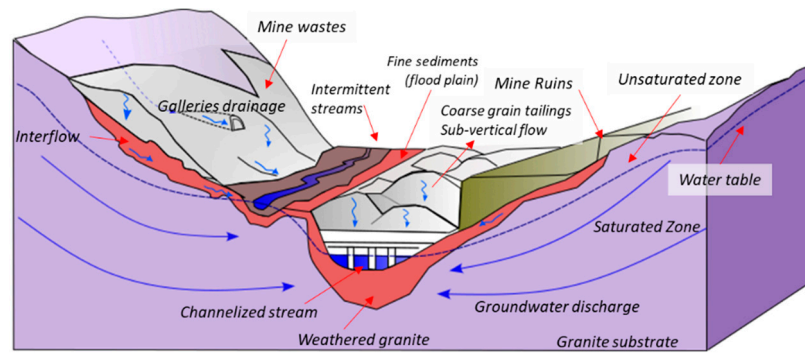


Figure 10. A hydrogeological conceptual model for the Regoufe mining area.

The hydrogeological profile creation process represents the final phase of the soil and subsurface survey. It combines the integration of information from field observations and geophysical results into sections of electrical, seismic, and electromagnetic data. In the absence of piezometric information, groundwater level data in wells, quantified porosity, and permeability information, the hydrogeological conceptual model represented in the following sections is highly interpretive and requires further research to be corroborated. However, as in many disciplines of Geosciences, the uncertainties inherent in such interpretations seek to be mitigated by the integration of different geophysical techniques and the use of analogous geological models, which will be explained in the following paragraphs.

In order to obtain a representative image of the mining area; four hydrogeological sections were made. Three of them are perpendicular to the axis of the valley where the mine is located (sections “A,” “B,” and “C”), and one section is parallel to the axis located in the central zone (section “D”), limited to the southern zone, where most of the mine waste deposits are located, the main objective of this work. Figure 11 illustrates the location of the hydrogeological sections and the electrical resistivity profiles.

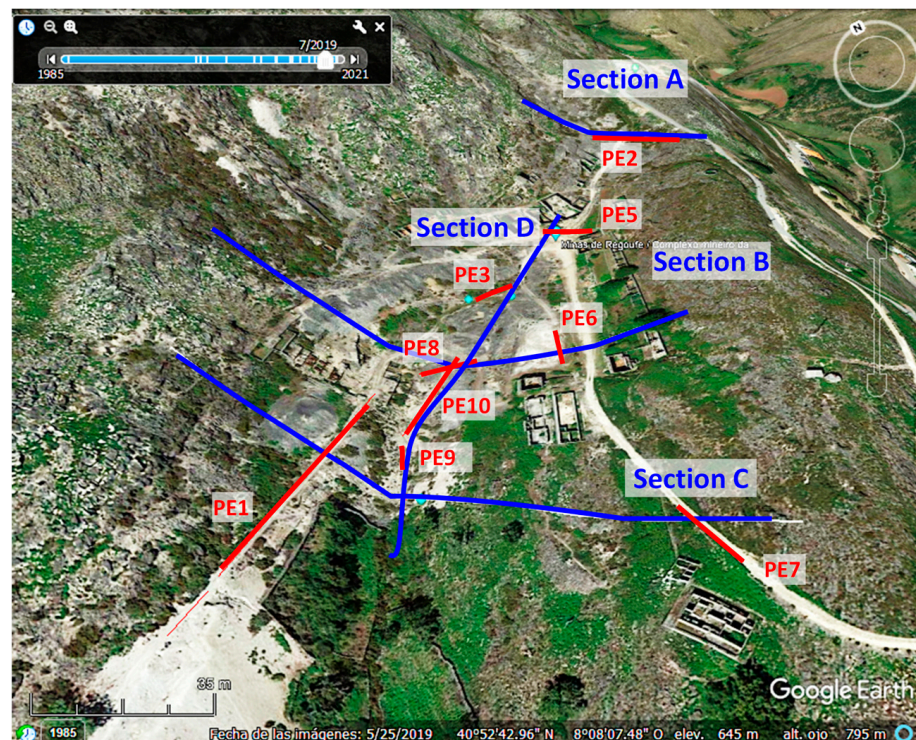


Figure 11. Location of hydrogeological sections and electrical profiles in a 3D overview with aerial photography extracted from Google Earth.

An example of the methodology is summarized in the workflow, and results are related in Section “D” (Figure 12). This section is one of the most important sections of the complex. It ran parallel to the valley axis and was defined from the largest amount of information available in the center of the valley and perpendicular to sections “B” and “C”. In particular, this key section allowed the integration of information from both seismic profiles PS1 and PS2, as well as the electrical profiles PE3, PE5, PE8, PE9, and PE10. It should be noted that, as well as the 2D “p” wave velocity profiles extracted from the seismic estimates, the “s” wave velocity and Young’s modulus (E) were also obtained, as explained in previous paragraphs. Similarly, following the same steps and based on the nearest geophysical and geological data available were constructed sections “A,” “B,” and “C,” as illustrated in Figure 13.

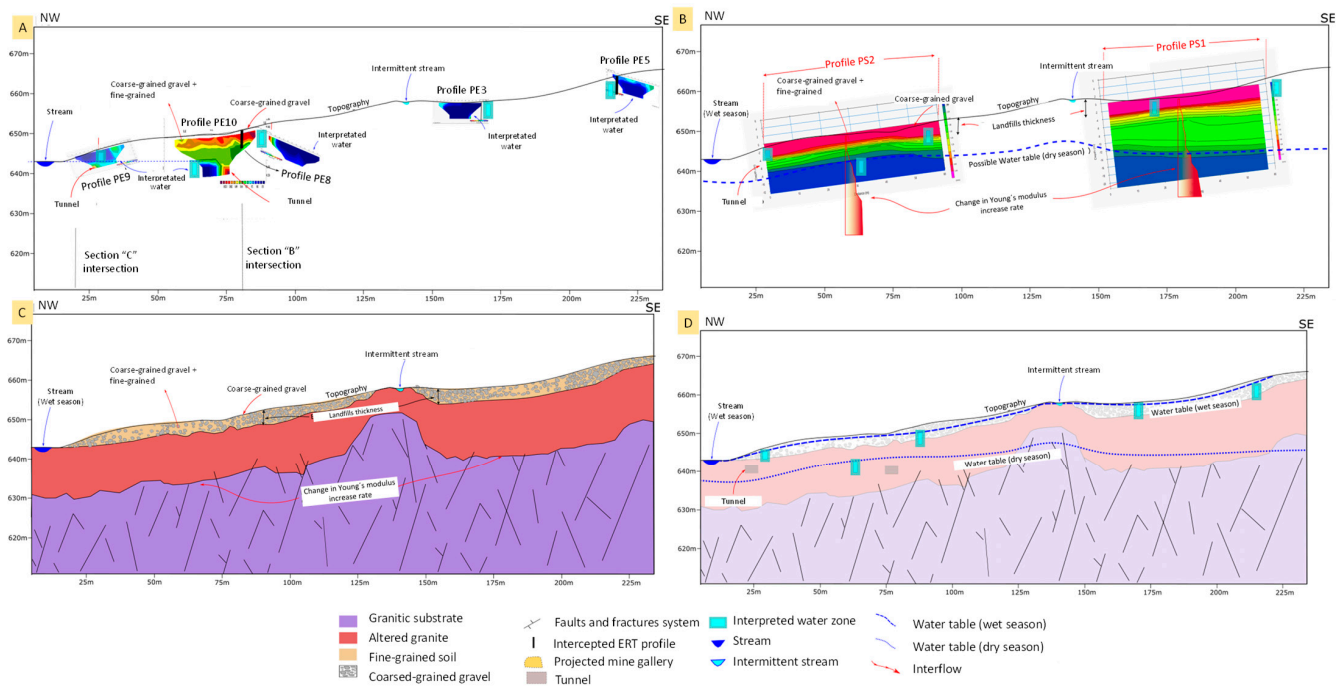


Figure 12. Hydrogeological interpretation process in Section “D” (see map location in Figure 9): (A) Data used and calibrated with surface observations (ERT profiles); (B) Seismic profiles results for PS1 and PS2 profiles (2D “p” wave velocity model and average Young’s Modulus E); (C) Geological interpretation; (D) Hydrogeological interpretation.

The hydrogeological interpretation considers the observations made in terms of the electrical and seismic responses of the subsurface and groundwater. With respect to the tailings material, a large deposit is expected on the slopes and valleys of the mining area.

In general, in geological terms and following analogous models [49], given the proximity of wetlands, a greater degree of alteration of the granitic body is expected towards the valleys due to greater contact with meteoric waters. Given the lack of seismic information in most of the area, the electrical profiles and their integration with soil thickness estimates from the seismic profiles PS1 and PS2 were used as a basis. The arrangement of fault and fracture planes is hypothetical, so the orientation of faults and fractures must be further validated with field studies to corroborate their geometric arrangement. Figure 12A shows the data corresponding to the electrical profiles as well as their subsurface interpretation in terms of soil type and interpreted water levels. Figure 12B shows the 2D seismic data of the compressional wave velocities (V_p) and Young’s modulus (E) profile at the center of the corresponding seismic profiles.

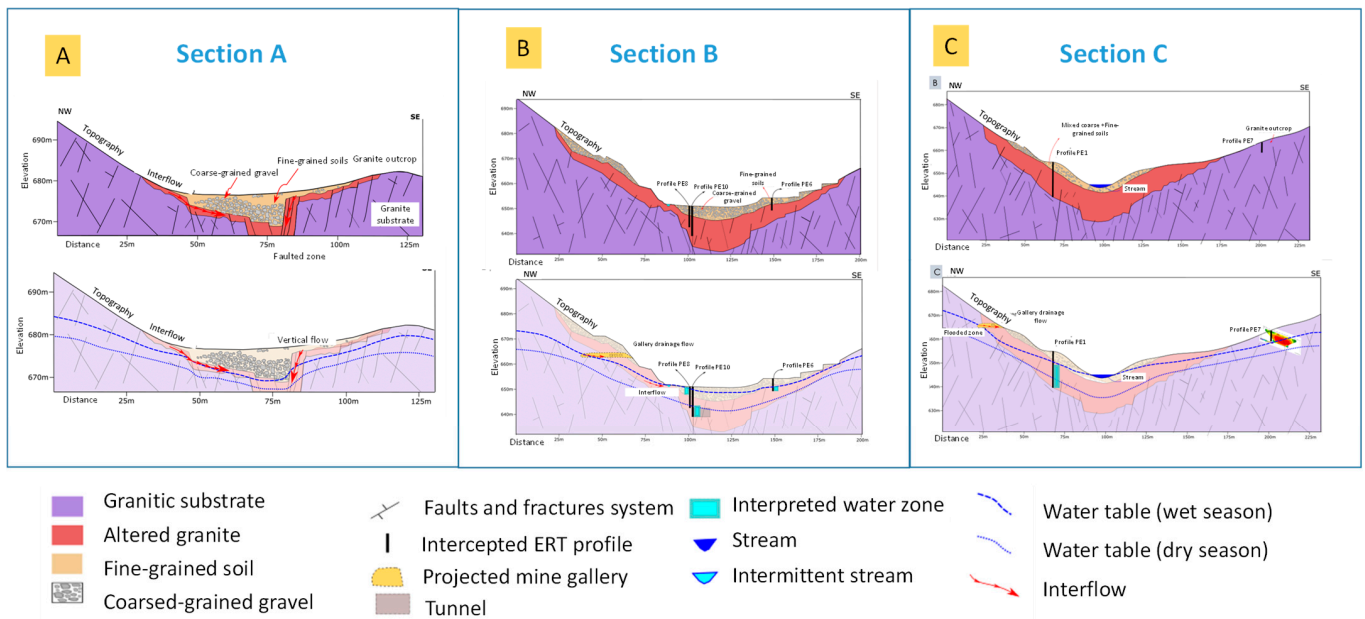


Figure 13. Geological and hydrogeological sections for wet and dry seasons respectively for (A) Section “A;” (B) Section “B;” (C) Section “C”. (See map location in Figure 11).

One of the most important pieces of information that can be extracted from this profile corresponds to the thickness data of the mine landfill soils, obtained from the seismic refraction information and corroborated with the MASW results. From this interpretation, an adjustment was made to the thicknesses in the remaining sections of the area, considering that the waste deposits could have an equivalent thickness in the other sections. Obviously, this is a rather conservative assumption, and future prospecting could improve the prediction in other areas (west and northeast of the mining area). Regarding the interpretation of the transition zone from weathered granite to harder bedrock, Young’s modulus was used, being equivalent in terms of depths in these profiles (15 m depth) (Figure 12B,C). Note that given the low quality of the MASW results, this interpretation should be considered with caution, and other techniques should be used for verification combined with these interpretations.

By integrating the information of possible water table depths obtained from the electrical profiles, the superficial run-off elevation, and the p-wave seismic information, it is observed that there is a good correlation at deep levels, which are interpreted as corresponding to the water table in this area (approximately 643 m a.s.l.). One of these observations is evident when comparing seismic sections PS1 and PS2 acquired on the same date, and therefore without seasonality effects on the water table (Figure 12B). In the deeper section, the change in compressional-wave velocity (V_p) from 1800 m/s to 2400 m/s is at about 640 m a.s.l. elevation. While the PS1 section, this change occurs slightly higher and at a consistently higher water table (645 m a.s.l.). It should be noted that in sediments of this nature, the air-water interface has a strong impact on the “p” wave, so it is often used to estimate the water table. In comparison, the velocity of the “s” wave remains unaffected by the presence of water and is but well affected by the mechanical parameters of the rock/soil. From this information and considering the highly water-saturated profiles (PE8, PE3, and PE5), the water table was defined for the wet season, and the results of the seismic information and profiles PE9 and PE10 as the levels corresponding to the dry season (Figure 12D).

5. Discussion

Finally, to visualize the spatial variations and correlate the observations highlighted here, a 3D model was made by means of interpolation techniques based on the resistivity data from the profiles and bounded by the topographic surface obtained from the digital terrain model (DME) (Figure 14). In order to keep the heterogeneities associated with this area, and as only data was available on the resistivity profiles, an Inverse Distance Anisotropic algorithm was used. The model shows the zones of higher resistivity in the higher zones, mainly associated with the granitic substrate, decreasing towards the central part of the valley. In the southeast area, a wetter and less resistive zone is interpreted. However, these zones were not evaluated and present a high uncertainty.

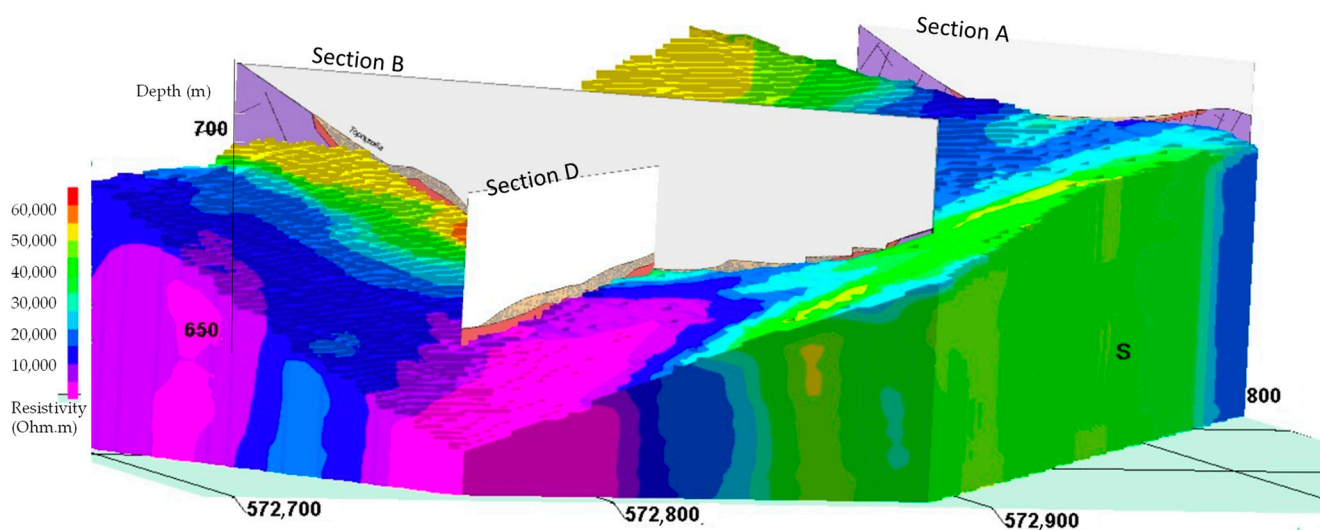


Figure 14. 3D visualization of the model of electrical resistivities and interpreted geological sections.

As for the hydrogeological model, the geometry of the water table assumes the conditions of a crystalline rock mass, low permeability and porosity, with a pronounced anisotropy due to the preferential orientation of faults and fractures, typical of this type of system. Thus, the phreatic surface, as discussed in the theoretical background of this chapter, is expected to be close to the surface and increasingly higher in the upper part of the massif and lower towards the valley areas until it reaches the discharge areas on the slopes. Since the galleries act as a strong drainage area, it is expected that in the areas close to the galleries, the water table will deepen. When we move away towards the granitic massif to the west, the phreatic surface rises. These observations are consistent with the EM data that was observed higher conductivities toward the east (Figure 5), where fewer galleries and consequently less drainage is interpreted as a closer water table in this zone. In the 3D electrical resistivity model, the blue-violet areas stand out, which are less resistive and therefore have a greater capacity for ionization. These are considered to be the areas with the greatest potential for contamination.

6. Conclusions

Integration of subsurface geophysical data and laboratory analyses allowed us to establish relationships between the electrical properties of the subsurface and observations in field soil and water samples. The electrical properties are characterized by low conductivity in soils of coarse-grained gravel deposits, fine-grained deposits of quartzitic nature, and in the granitic substrate. Conversely, high conductivity exists in areas of high-water saturation associated with subsurface flow zones or as a response from the phreatic surface.

Geophysical integration using techniques such as seismic refraction and MASW allowed better characterization of the thickness of the mine waste deposits, differentiation of the granitic zone of major alteration, and depth of the unweathered granitic substrate. In addition to the definition of the phreatic surface in the central valley. As part of the objectives of this project, electrical conductivity (EM) and electrical resistivity (ERT) maps were generated. In the case of EM, the maps appear to reflect a higher elevation of the phreatic surface on the eastern side of the mine valley. In contrast to the western area, where the conductivity is relatively lower. In the latter region, this phenomenon may be associated with higher drainage due to the large number of tunnels and galleries present. While the resistivity maps (ERT) reflect a central area of the mine valley with values of about 1000 Ωm . These values, compared to the laboratory analysis using mineralized water, are much higher, indicating a low probability of occurrence of ionized water and, therefore, low levels of contamination.

Four hydrogeological sections, a 3D model of electrical resistivities, and a conceptual hydrogeological model were constructed to characterize the mine waste deposits and hypothetical water tables. Despite the high uncertainty in regions of crystalline systems, this type of integrated modeling provides a basis for future, more detailed analyses of the hydrogeological system around the mining area. In addition to defining appropriate environmental intervention work, such as soil remediation and treatment of potentially contaminated water.

Author Contributions: Conceptualization, H.D.A. and H.S.; Methodology, H.D.A., R.M. and J.E.M.; Software, H.D.A. and R.M.; Validation, H.S. and R.M.; Formal analysis, H.D.A.; Investigation, H.D.A., H.S., R.M. and J.E.M.; Resources, H.S.; Data curation, H.D.A., M.C.G.M. and J.E.M.; Writing—original draft, H.D.A.; Writing—review & editing, H.D.A., H.S., R.M. and J.E.M.; Supervision, H.S. and R.M.; Project administration, H.S. All authors have read and agreed to the published version of the manuscript.

Funding: This research was supported by the “SHS: Soil health surrounding former mining areas: characterization, risk analysis, and intervention” Project, financed by NORTE-45-2020-75-SISTEMA DE APOIO À INVESTIGAÇÃO CIENTÍFICA E TECNOLÓGICA-“PROJETOS ESTRUTURADOS DE I&D”-HORIZONTE EUROPA, Ref. NORTE-01-0145-FEDER-000056 and framed within the ICT G3 activities (UIDB/04683/2020 and UIDP/04683/2020).

Data Availability Statement: This research is part of a master’s thesis that, at the time of this publication, has not yet been fully completed. The data would be available in: De Almeida, H. Integração de metodologias geofísicas na avaliação do impacto ambiental no subsolo da Mina de Regoufe—Arouca. Master’s thesis (Unpublished master’s thesis). Porto University, Porto, Portugal, 2023.

Conflicts of Interest: The authors declare no conflict of interest.

Appendix A

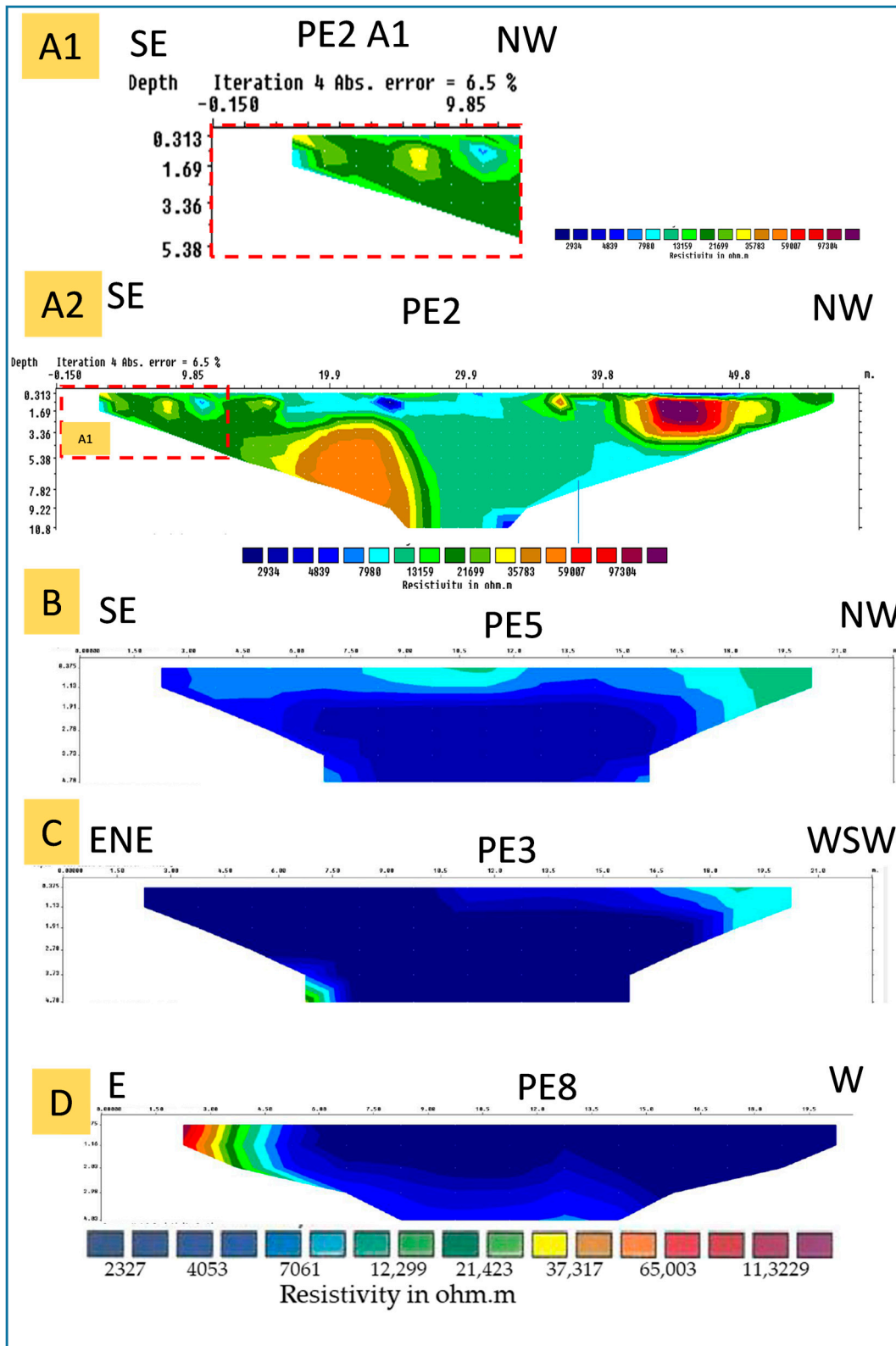


Figure A1. True electrical resistivity profiles (ERT) transverse to the valley axis. (A1) Profile PE2, which corresponds to the magnified image of the SE part of profile PE2 at the same scale as profile PE5 for easy comparison and interpretation. (A2) Profile PE2; (B) Profile PE5; (C) Profile PE3; (D) Profile PE8. For location, look at Figure 3.

Appendix B

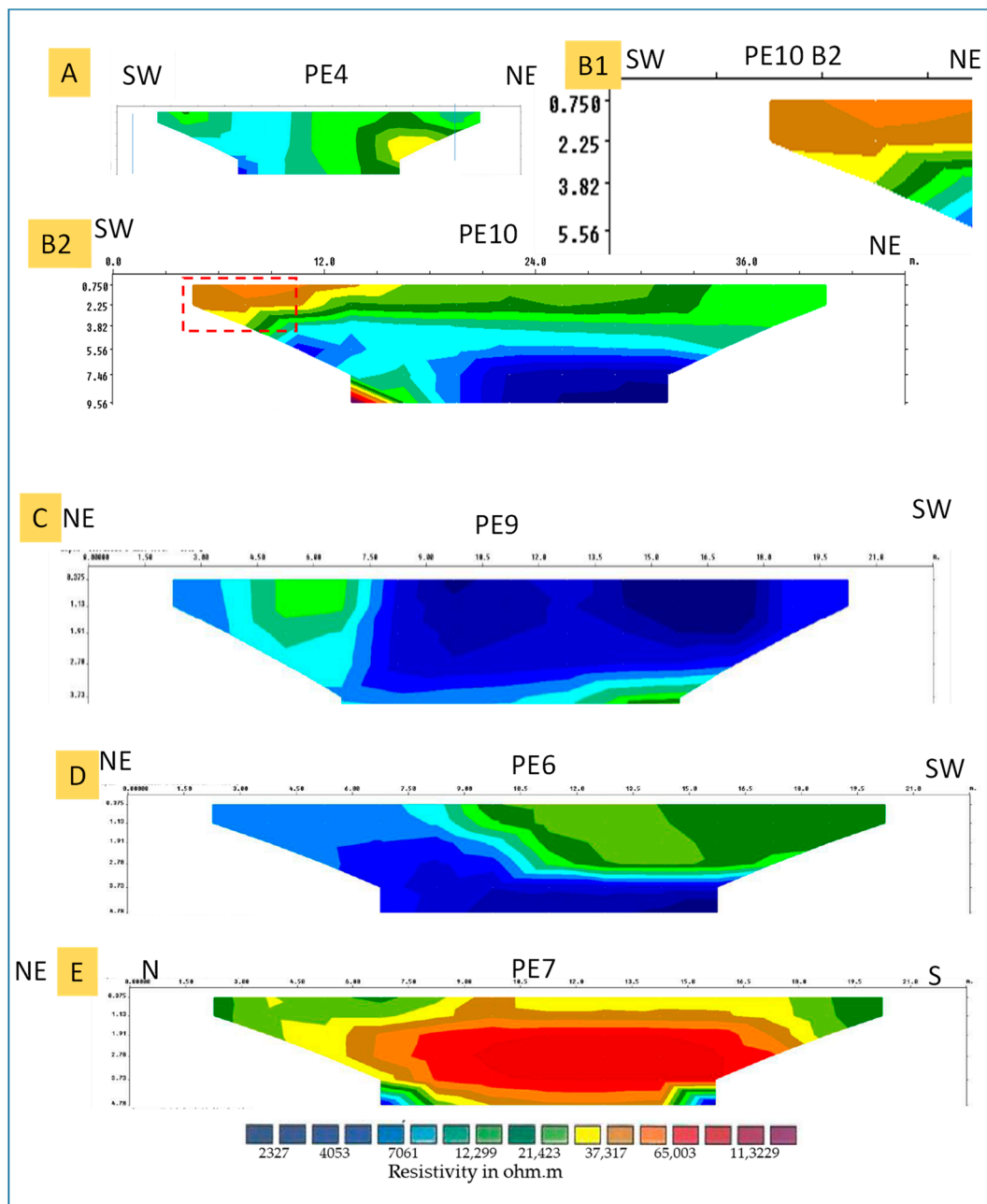


Figure A2. True electrical resistivity profiles (ERT) parallel to the mountain slopes. (A) Profile PE4, (B1) PE10 region, which corresponds to the magnified image of the SW part of PE10 at the same scale as profile PE4 for easy comparison and interpretation; (B2) Profile PE10; (C) Profile PE9; (D) Profile PE6; (E) Profile PE7. For the location, look at Figure 3.

References

1. Correia, V.F.; Favas, P.J.C.; Sá, A. *Impacto das Drenagens Ácidas das Minas de Regoufe e Rio de Frades (Geoparque Arouca) na Qualidade de Água Superficial*; Centro de Estudos Clássicos e Humanísticos da Universidade de Coimbra: Coimbra, Portugal, 2012.
2. Durães, N.; Portela, L.; Sousa, S.; Patinha, C.; Silva, E. Environmental Impact Assessment in the Former Mining Area of Regoufe (Arouca, Portugal): Contributions to Future Remediation Measures. *Int. J. Environ. Res. Public Heal.* **2021**, *18*, 1180. [[CrossRef](#)] [[PubMed](#)]
3. Favas, P.; Sarkar, S.; Rakshit, D.; Venkatachalam, P.; Prasad, M. *Acid Mine Drainages From Abandoned Mines: Hydrochemistry, Environmental Impact, Resource Recovery, and Prevention of Pollution, Environmental Materials and Waste*; Academic Press: Cambridge, MA, USA, 2016; Chapter 17; pp. 413–462.

4. Sousa, S.C. *Avaliação do Impacte Ambiental das Minas de Volfrâmio de Regoufe—Arouca*; Departamento de Geociências, Universidade de Aveiro: Aveiro, Portugal, 2016; p. 115.
5. Candeias, C.; Da Silva, E.F.; Salgueiro, A.R.; Pereira, H.G.; Reis, A.P.; Patinha, C.; Matos, J.X.; Ávila, P.H. Assessment of soil contamination by potentially toxic elements in the aljustrel mining area in order to implement soil reclamation strategies. *Land Degrad. Dev.* **2011**, *22*, 565–585. [[CrossRef](#)]
6. González, I.; Galán, E.; Romero, A. Assessing Soil Quality in Areas Affected by Sulfide Mining. Application to Soils in the Iberian Pyrite Belt (SW Spain). *Minerals* **2011**, *1*, 73–108. [[CrossRef](#)]
7. Martínez, J.; Rey, J.; Hidalgo, M.C.; Benavente, J. Characterizing Abandoned Mining Dams by Geophysical (ERI) and Geochemical Methods: The Linares-La Carolina District (Southern Spain). *Water Air Soil Pollut.* **2012**, *223*, 2955–2968. [[CrossRef](#)]
8. Patinha, C.; da Silva, E.F.; Fonseca, E.C. Mobilisation of arsenic at the Talhadas old mining area—Central Portugal. *J. Geochem. Explor.* **2004**, *84*, 167–180. [[CrossRef](#)]
9. Lottermoser, B.G. Sulfidic Mine Wastes. In *Mine Wastes: Characterization, Treatment, Environmental Impacts*; Springer: Berlin, Germany, 2007; pp. 33–87.
10. Eary, L.; Runnells, D.D.; Esposito, K. Geochemical controls on ground water composition at the Cripple Creek Mining District, Cripple Creek, Colorado. *Appl. Geochem.* **2003**, *18*, 1–24. [[CrossRef](#)]
11. Paschke, S.S.; Harrison, W.J.; Walton-Day, K. Effects of acidic recharge on groundwater at the St. Kevin Gulch site, Leadville, Colorado. *Geochem. Explor. Environ. Anal.* **2001**, *1*, 3–14. [[CrossRef](#)]
12. Lachmar, T.E.; Burk, N.I.; Kolesar, P.T. Groundwater Contribution of Metals from an Abandoned Mine to The North Fork of The American Fork River, Utah. *Water Air Soil Pollut.* **2006**, *173*, 103–120. [[CrossRef](#)]
13. Rocha, D.; Brilha, J.; Sá, A. *Inventariação e a Avaliação do Património Geológico na Fundamentação Científica do Geoparque Arouca (Norte de Portugal)*; Memórias e Notícias—Publicação do Departamento Ciências Terra e do Museu Mineralogia e Geologia da Universidade de Coimbra: Coimbra, Portugal, 2008; p. 3.
14. Reynolds, J.M. *An Introduction to Applied and Environmental Geophysics*; John Wiley & Sons: Hoboken, NJ, USA, 2011.
15. Fontoura, M.; Moura, R.; Dias, A. A Geologia e a Geofísica na avaliação da contaminação associada a Vazadouros Controlados-o caso do VC de Matosinhos no Norte de Portugal. *Comun. Geol.* **2011**, *98*, 83–92.
16. Wagner, F.M.; Uhlemann, S. *Chapter One—An overview of multimethod imaging approaches in environmental geophysics*, In *Advances in Geophysics*; Schmelzbach, C., Ed.; Elsevier: Amsterdam, The Netherlands, 2021; pp. 1–72.
17. Casagrande, M.F.S.; Moreira, C.A.; Targa, D.A.; Alberti, H.L.C. Integration of Geophysical Methods in the Study of Acid Drainage in Uranium Mining Waste. *Braz. J. Geophys.* **2018**, *36*, 439–450. [[CrossRef](#)]
18. Robles Arenas, V.; Candela Lledó, L. Hydrological conceptual model characterisation of an abandoned mine site in semiarid climate: The Sierra de Cartagena-La Unión (SE Spain). *Geol. Acta* **2010**, *8*, 235–248.
19. Schmidt, S.E.A. *Hydrologic evaluation of plugging Dinero Tunnel to improve water quality in Lake Fork Creek, Leadville, CO. 2000–2009*; Mines Theses & Dissertations, Master of Science, Colorado School of Mines: Golden, CO, USA, 2007.
20. Carrington da Costa, J. *Notícia Sobre uma Carta Geológica do Buçaco, de Nery Delgado*; Direcção Geral de Minas e Serviços Geológicos, Serviços Geológicos de Portugal: Lisboa, Portugal, 1950.
21. Teixeira, C. *Notas Sobre Geologia de Portugal: O Complexo Xisto-Grauwáquico Ante-Ordoviciano*; Empresa Literaria Fluminense: Lisboa, Portugal, 1955.
22. Ortega Gironés, E.; Hernández Urroz, J.; González Lodeiro, F. *Distribución Paleogeográfica y Control Estructural de los Materiales Anteordovícicos en la Parte Suroriental del Autóctono de la Zona Centroibérica*; Congreso geológico de España: Granada, Spain, 1988; p. 2.
23. Ribeiro, A.; Silva, J.B.; Dias, R.; Pereira, E.; Oliveira, J.T.; Rebelo, J.; Romão, J.; Silva, A.F. Sardinian inversion tectonics in the Centro-Iberian Zone. In *III Congresso Nac. Geol. Resumos*; Generalista: Coimbra, Portugal, 1991.
24. Brun, J.-P.; Burg, J.-P. Combined thrusting and wrenching in the Ibero-Armorican arc: A corner effect during continental collision. *Earth Planet. Sci. Lett.* **1982**, *61*, 319–332. [[CrossRef](#)]
25. Matte, P. Tectonics and plate tectonics model for the Variscan belt of Europe. *Tectonophysics* **1986**, *126*, 329–374. [[CrossRef](#)]
26. Matte, P. The Variscan collage and orogeny (480–290 Ma) and the tectonic definition of the Armorica microplate: A review. *Terra Nova* **2001**, *13*, 122–128. [[CrossRef](#)]
27. Matte, P.; Ribeiro, A. Forme et orientation de la virgation hercynienne de Galice. Relations avec le plissement et hypothèses sur la genèse de l’arc Ibero-Armoricain. *Cr Seances Acad. Sci. Paris* **1975**, *280*, 2825–2828.
28. Ribeiro, A.; Pereira, E.; Severo, L. *Análise da Deformação da Zona de Cisalhamento Porto-Tomar na Transversal de Oliveira de Azeméis*; Comunicações dos Serviços Geológicos de Portugal: Lisboa, Portugal, 1980.
29. Vera, J.A. *Geología de España*; Igme: Madrid, Spain, 2004; p. 884.
30. Pinto, M.C.S.; Martín, C.C.; Ibarrola, E.; Castañón, L.G.C.; Portugal-Ferreira, M.R. Síntese geocronológica dos granitóides do Maciço Hespérico. In *Geología de los granitoides y rocas asociadas del Macizo Hespérico Libro Homenaje a L.C. García de Figuerola*; Editorial Rueda: Madrid, Spain, 1987.
31. Vriend, S.P.; Oosterom, M.G.; Bussink, R.W.; Jansen, J.B.H. Trace-element behavior in the W-Sn granite of Regoufe, Portugal. *J. Geochem. Explor.* **1985**, *23*, 13–25. [[CrossRef](#)]
32. Sluijk, D. *Geology and Tin-tungsten Deposits of the Regoufe Area, Northern Portugal*; Universiteit van Amsterdam: Amsterdam, The Netherlands, 1963.

33. Tavares, J.I. *Geologia da Região de Regoufe*, in *Departamento de Geociências*; Universidade de Aveiro: Aveiro, Portugal, 2006; p. 142.
34. Pereira, E. *Notícia Explicativa da Folha 13-D Oliveira de Azeméis*; INETI Instituto Nacional de Engenharia: Lisboa, Portugal, 2007.
35. Van Gaans, P.; Vriend, S.; Poorter, R. Hydrothermal processes and shifting element association patterns in the W—Sn enriched granite of Regoufe, Portugal. *J. Geochem. Explor.* **1995**, *55*, 203–222. [[CrossRef](#)]
36. Favas, P.J.C. *Biogeoquímica em áreas minerais estano-volframíticas. Tese de Doutoramento*; Universidade de Trás-os-Montes e Alto Douro: Vila Real, Portugal, 2008; p. 805.
37. Favas, P.J.C.; Pratas, J.; Gomes, M.E.P. *Hidroquímica das águas superficiais na área mineira de Regoufe (Arouca, Norte de Portugal)*, In *VIII Congresso Nacional de Geologia*; Revista Electrónica de Ciências da Terra Geosciences On-line Journal: Lisboa, Portugal, 2010.
38. Marques, M.C. *Contribuição da Resistividade Elétrica na Avaliação Ambiental do Subsolo da Zona Envolvente à Mina de Regoufe, Arouca, Portugal*; Departamento de Geociências Ambiente e Ordenamento do Território, Universidade do Porto: Porto, Portugal, 2019; p. 56.
39. Figueiredo, F.; Catarino, L. Prospecção de recursos hídricos em meio cristalino por métodos geofísicos. Caso de estudo da Senhora do castelo (Mangualde). In *11 Seminário Sobre Águas Subterrâneas*; Instituto Superior de Engenharia do Porto: Porto, Portugal, 2017; p. 6.
40. Telford, W.M.; Geldart, L.P.; Sheriff, R. *Applied Geophysics*; Cambridge University Press: Cambridge, UK, 1990.
41. Palacky, G. Resistivity Characteristics of Geologic Targets. *Electromagn. Methods Appl. Geophys.* **1988**, *1*, 53–129.
42. Bergmann, P.; Ivandic, M.; Norden, B.; Rucker, C.; Kiessling, D.; Luth, S.; Schmidthattenberger, C.; Juhlin, C. Combination of seismic reflection and constrained resistivity inversion with an application to 4D imaging of the CO₂ storage site, Ketzin, Germany. *GEOPHYSICS* **2014**, *79*, B37–B50. [[CrossRef](#)]
43. Carvalho, J.M.; Chaminé, H.; Afonso, M.J.; Espinha Marques, J.M.; Medeiros, A.; Garcia, S.; Gomes, A.A.; Teixeira, J.; Fonseca, P. *Productivity and Water Costs in Fissured-Aquifers from the Iberian Crystalline Basement (Portugal)*; Hydrogeological Constraints: Porto, Portugal, 2005.
44. Chalise, S. High mountain hydrology in changing climates: Perspectives from the Hindu Kush-Himalayas. Developments in hydrology of mountain areas. In *Proceedings of FRIEND AMHY Annual Report*; UNESCO: New York, NY, USA, 1997; pp. 23–31.
45. Gurtz, J.; Zappa, M.; Jasper, K.; Lang, H.; Verbunt, M.; Badoux, A.; Vitvar, T. A comparative study in modelling runoff and its components in two mountainous catchments. *Hydrol. Process.* **2003**, *17*, 297–311. [[CrossRef](#)]
46. Marques, J.E.; Carreira, P.M.; Graça, R.C.; Aires-Barros, L.; Carvalho, J.M.; Chaminé, H.; Borges, F.S. Geothermal fluids circulation at Caldas do Moledo area, Northern Portugal: Geochemical and isotopic signatures. *Geofluids* **2003**, *3*, 189–201. [[CrossRef](#)]
47. Marques, J.; Santos, M.F.; Graça, R.; Castro, R.; Aires-Barros, L.; Mendes Victor, L. A geochemical and geophysical approach to derive a conceptual circulation model of CO₂-rich mineral waters: A case study of Vilarelho da Raia, northern Portugal. *Hydrogeol. J.* **2001**, *9*, 584–596.
48. Offerdinger, U.S.; Balderer, W.; Loew, S.; Renard, P. Environmental isotopes as indicators for ground water recharge to fractured granite. *Ground Water* **2004**, *42*, 868–879. [[PubMed](#)]
49. Lubczynski, M.W.; Gurwin, J. Integration of various data sources for transient groundwater modeling with spatio-temporally variable fluxes—Sardon study case, Spain. *J. Hydrol.* **2005**, *306*, 71–96. [[CrossRef](#)]

Disclaimer/Publisher’s Note: The statements, opinions and data contained in all publications are solely those of the individual author(s) and contributor(s) and not of MDPI and/or the editor(s). MDPI and/or the editor(s) disclaim responsibility for any injury to people or property resulting from any ideas, methods, instructions or products referred to in the content.